RESEARCH ARTICLE

Macromolecular Bioscience
www.mbs-journal.de

Enhancing Hemocompatibility in ECMO Systems With a Fibrinolytic Interactive Coating: in Vitro Evaluation of Blood Clot Lysis Using a 3D Microfluidic Model

Lena Witzdam, Samarth Sandhu, Suji Shin, Yeahwa Hong, Shanzeh Kamal, Oliver Grottke, Keith E. Cook, and Cesar Rodriguez-Emmenegger**

Blood-contacting medical devices, especially extracorporeal membrane oxygenators (ECMOs), are highly susceptible to surface-induced coagulation because of their extensive surface area. This can compromise device functionality and lead to life-threatening complications. High doses of anticoagulants, combined with anti-thrombogenic surface coatings, are typically employed to mitigate this risk, but such treatment can lead to hemorrhagic complications. Therefore, bioactive surface coatings that mimic endothelial blood regulation are needed. However, evaluating these coatings under realistic ECMO conditions is both expensive and challenging. This study utilizes microchannel devices to simulate ECMO fluid dynamics and assess the clot-lysis efficacy of a self-activating fibrinolytic coating system. The system uses antifouling polymer brushes combined with tissue plasminogen activator (tPA) to induce fibrinolysis at the surface. Here, tPA catalyzes the conversion of blood plasminogen into plasmin, which dissolves clots. This positive feedback loop enhances clot digestion under ECMO-like conditions. This findings demonstrate that this coating system can significantly improve the hemocompatibility of medical device surfaces.

1. Introduction

Blood-contacting medical devices with large surface areas, such as extracorporeal membrane oxygenators (ECMOs), rapidly trigger surface-induced coagulation, resulting in device failure and thromboembolic complications.[1–3] To mitigate these issues, antithrombotic surface coating strategies have been developed to enhance the hemocompatibility of such devices,[4–7] including surface passivation,[8–23] heparin coatings,[24–28] immobilization of thrombin inhibitors,[29–33] and NO-releasing substrates.[34,35] A notable example is the design of an endothelium-inspired strategy that activates the body's own fibrinolytic system, thereby reducing clot formation.[36] This interactive coating system is inspired by the endothelium's natural antithrombotic mechanisms.[37–40] This system is designed to be non-thrombogenic in its dormant state but can detect fibrin from a thrombus and switch to an active state. In the active state, it utilizes the body's fibrinolytic pathway to locally disintegrate the thrombus, then returns to its dormant state without disrupting overall hemostasis.[36] The non-thrombogenic state is achieved by antifouling polymer brushes based on *N*-(2-hydroxypropyl) methacrylamide (HPMA) and carboxybetaine methacrylamide (CBMAA) that prevent plasma protein and cell adsorption.[36] Fibrinolytic activity

L. Witzdam, C. Rodriguez-Emmenegger
Institute for Bioengineering of Catalonia (IBEC)
The Barcelona Institute of Science and Technology (BIST)
Carrer de Baldiri Reixac, 10, 12, Barcelona 08028, Spain
E-mail: rodriguez@dwi.rwth-aachen.de

L. Witzdam, C. Rodriguez-Emmenegger
DWI – Leibniz Institute for Interactive Materials
Forckenbeckstr. 50, 52074 Aachen, Germany

L. Witzdam
Institute of Technical and Macromolecular Chemistry
RWTH Aachen University
Worringerweg 2, 52074 Aachen, Germany

The ORCID identification number(s) for the author(s) of this article can be found under https://doi.org/10.1002/mabi.202400530

DOI: 10.1002/mabi.202400530

S. Sandhu, S. Shin, Y. Hong, S. Kamal, K. E. Cook
Department of Biomedical Engineering
Carnegie Mellon University
5000 Forbes Ave, Pittsburgh, PA 15213, USA
E-mail: keicook@andrew.cmu.edu

O. Grottke
Department of Anesthesiology
RWTH Aachen University Hospital
Pauwelsstr. 30, 52074 Aachen, Germany

C. Rodriguez-Emmenegger
Institució Catalana de Recerca i Estudis Avançats (ICREA)
Passeig Lluís Companys 23, Barcelona 08010, Spain

C. Rodriguez-Emmenegger
Biomedical Research Networking
Center in Bioengineering
Biomaterials and Nanomedicine
The Institute of Health Carlos III
Av. Monforte de Lemos 3–5, Madrid 28029, Spain

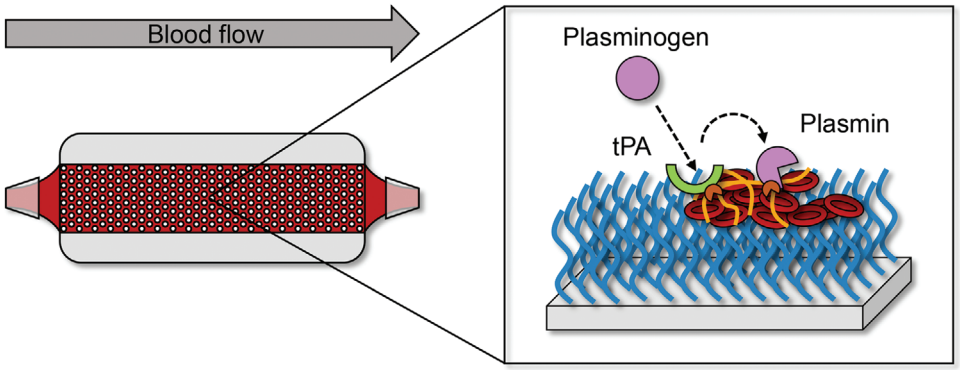

Figure 1. Experimental design utilized to test the hemocompatibility of the fibrinolytic nanocoating in conditions mimicking ECMO. Left: Scheme of 3D printed microchannel devices. The grey dots depict small pillars that force changes in flow and increase of tortuosity for blood. The arrow on top indicates the flow direction of blood. Right: Scheme of the surface, illustrating the coating and its principle of action, based on the local activation of the fibrinolytic system by tPA covalently attached to brushes.

is introduced by decorating these brushes with tissue plasminogen activator (tPA) that converts plasminogen into plasmin, the enzyme that breaks down fibrin.[41,42] The coating system incorporates feedback mechanisms that regulate fibrinolysis. The immobilization of tPA on the surface protects it from inhibitors and enhances its activity in the presence of fibrin.[36] This interaction significantly increases tPA's affinity for plasminogen, switching the coating to its active state.[37,38,41,42] In this state, plasmin production is continuous, favoring fibrin digestion over inhibition due to plasmin's high affinity for fibrin.[41] This system ensures the complete digestion of thrombi and a return to the dormant state, with residual plasmin being neutralized to avoid affecting hemostasis.[37,38,41] While this coating strategy has shown promising results in contact with human blood under static conditions,[36] its performance under fluid-dynamic conditions that closely mimic real ECMO environments remains untested. The challenge lies in the requirement for large volumes of blood to accurately assess hemocompatibility in ECMO-like conditions, which is impractical for routine testing. Long-term experiments to determine clot formation are time-consuming, costly, and require numerous animals due to variability. Therefore, further research is needed to understand clot initiation and progression in fiber bundles under controlled conditions. These insights could aid in examining the efficacy of surface coatings in reducing clotting and extending device functionality. Lai et al. investigated the effects of fiber bundle path length, packing density, and blood flow velocity on clot formation and platelet/fibrin localization.[43,44] In this work, we use a 3D-printed microchannel device that mimics fiber bundle fluid mechanics, and high-throughput, cost-effective experiments were conducted. This setup consists of a small chamber (20 mm x 7.3 mm x 3 mm) that has pillars that break the flow of blood. This design, while very different than hollow fibers, best accounts for the different changes in direction and tortuosity that can be found in oxygenators and it is superior to a scale-down mini-ECMO. Human blood was pumped through these devices for 15 min, monitoring clot formation via blood flow resistance testing and quantifying clot volume with post-experiment imaging.[44] While the device material differs from the typical fiber material, it is similar to polyurethanes used in artificial lung housings. This setup can be used to evaluate the impact of the tPA-coating on clot formation in low-shear stress environments without the need for high volumes of blood. This innovative approach allows for a more feasible and practical assessment of hemocompatibility.

In this study, we investigate the effectiveness of tPA-decorated polymer brushes in enhancing hemocompatibility and promoting clot lysis within these microchannel devices. We achieved this by functionalizing the surfaces of the microchannel devices with tPA-decorated polymer brushes, subsequently perfusing blood through the devices, and evaluating clot formation using micro-computed tomography. This approach provides a more accurate simulation of ECMO conditions, enabling a better assessment of the coating's performance in real-world applications (**Figure 1**).

2. Results and Discussion

2.1. Modification of Microchannel Device with tPA-Coating

The successful modification of the microchannel devices with poly(HPMA-*co*-CBMAA) brushes was confirmed by X-ray photoelectron spectroscopy (XPS) analysis as illustrated in **Figures 2** and S1 (Supporting Information) and Table S1 (Supporting Information). The spectra obtained from the C1s region show C—C, C—H components at 285.0 eV, primarily attributed to the device. The C1s spectrum of the bare device additionally displays signals for the C—O component at 286.7 eV and O—C=O component at 289.3 eV, corresponding to the acrylate composition of the bare device. In contrast, the C1s spectrum of the device functionalized with polymer brushes exhibits additional peaks indicative of the incorporation of HPMA and CBMAA moieties. Specifically, contributions from C—N bonds at 285.7 eV and C—O bonds at 286.6 eV were observed, reflecting the presence of HPMA and CBMAA, respectively. Moreover, the methacrylamide backbone of HPMA and CBMAA arises at 288.1 eV. The carboxylic group of CBMAA was represented by the O—C=O component at 289.3 eV. Additionally, as anticipated, only the device functionalized with polymer brushes displayed signals in the N1s region. A peak at 399.0 eV was assigned to the amide group of HPMA and CBMAA, while another peak at 401.4 eV originated from the positively charged nitrogen of the quaternary ammonium group in CBMAA. Notably, the intensity of the signal at 399.0 eV

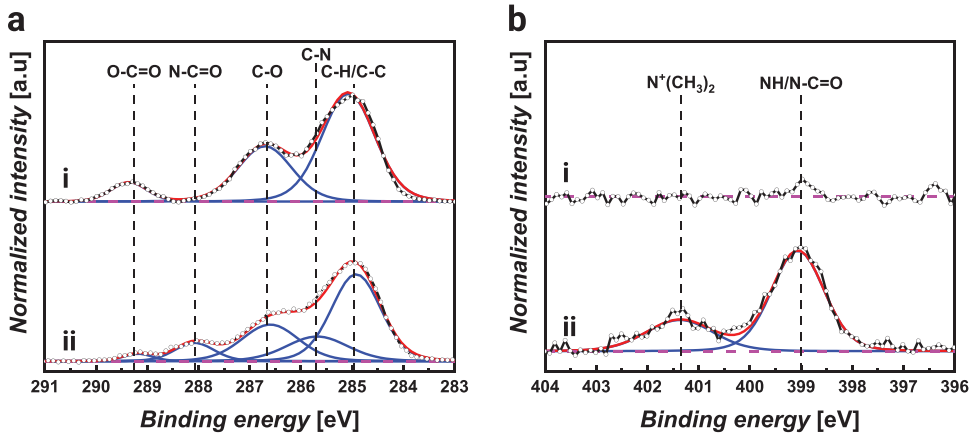

Figure 2. High-resolution XPS a) C1s and b) N1s spectra of i) bare microchannel devices and ii) microchannel devices functionalized with poly(HPMA-*co*-CBMAA) brushes.

exceeded that at 401.4 eV, indicating a higher proportion of HPMA in the copolymerization compared to CBMAA. The thickness of the brushes is in the range of 30–40 nm, which allows for sufficient antifouling properties without impairing the shape of the microchannel devices.

Additionally, the immobilization of tPA onto a microchannel device functionalized with polymer brushes and the remaining antifouling properties were evaluated by surface plasmon resonance spectroscopy (SPR) on a model surface. The model surface was generated by spin-coating the resin, which is used for 3D printing, on a SPR-chip followed by UV irradiation to allow cross-linking. The resin layer exhibits a thickness of 10 ± 1.7 nm. The produced model surface is then functionalized with polymer brushes and the immobilization of tPA is followed in real-time by SPR (**Figure 3a**). The SPR sensogram shows a successful immobilization of tPA with Γ_{tPA} = 35.7 ng·cm^{-2} (Table S2 in the SI, n = 3). It should be noted that tPA is immobilized by an amide bond that is stable under the shear conditions. The contact of blood plasma (BP) with the tPA-functionalized brushes resulted in a fouling $\Gamma_{BP\ proteins}$ = 65.5 ng·cm^{-2} (Figure 3b and Table S3 in the SI) which is only 20% of the fouling on the bare resin $\Gamma_{BP\ proteins}$ = 324 ng·cm^{-2} and represents less than 6% difference to the fouling observed on brushes without tPA.

2.2. Evaluation of Enzymatic Activity in Microchannel Devices

Bare microchannel devices, devices modified with polymer brushes, and devices modified with tPA-functionalized polymer brushes were contacted with undiluted BP for 30 min to determine the fibrinolytic activity through the formation of D-Dimers as a byproduct during clot lysis (**Figure 4a**). This experiment is independent. Bare devices and devices modified with polymer brushes had comparable levels of D-Dimer concentration, but the devices modified with tPA-functionalized polymer brushes showed an increase in the D-Dimer concentration by 239% (Figure 4b). This indicates that immobilized tPA can digest fibrin clots that are formed during contact with BP in the microchannel device, demonstrating the enzymatic activity of tPA.

2.3. Clot Formation in Microchannel Devices

Clot formation was evaluated using slightly heparinized whole human blood (0.06 U·mL^{-1}), which was pumped through the microchannel devices at a flow rate of 3 mL·min^{-1} for 15 min. This time is sufficiently long for fouling and activation events to occur (see section of fouling) while not requiring

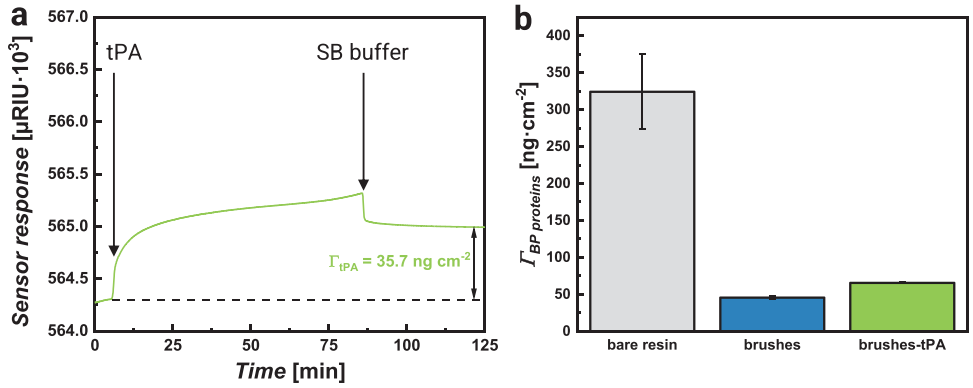

Figure 3. a) Selected SPR-sensogram of the immobilization of tPA on model surface followed in real-time by SPR confirming the successful modification of microchannel devices with tPA-functionalized brushes. b) Evaluation of antifouling properties before and after tPA-functionalization. n = 3.

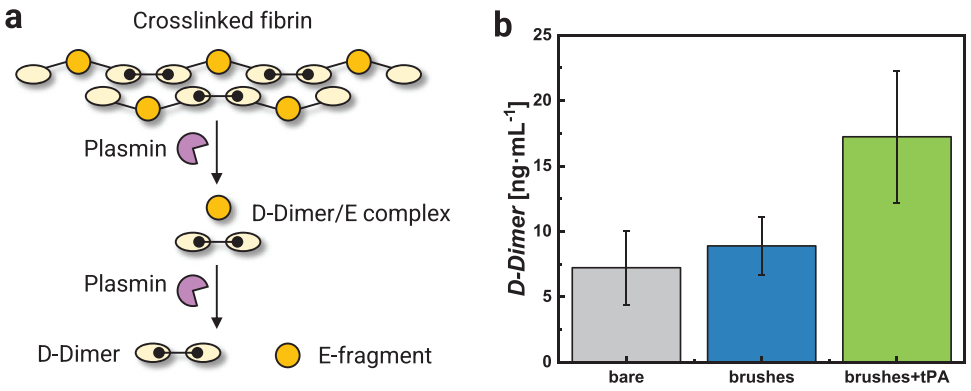

Figure 4. Evaluation of fibrinolytic activity by tPA. a) Scheme of the fibrin digestion by plasmin and the corresponding degradation products. b) D-Dimer concentration of BP samples after contact (30 min) with the bare device, the device coated with polymer brushes, and the devices coated with tPA-functionalized brushes. n = 3.

stronger anticoagulation as needed for longer experiments and that would otherwise obscure the evaluation of the antifouling and fibrinolytic activity of the coating. Simultaneously, flow resistance data was recorded versus time. **Figure** 5a demonstrates that clot formation is mildly delayed in microchannel devices modified with polymer brushes compared to the bare device. An even greater delay is observed in devices modified with tPA-functionalized polymer brushes. Device resistance was significantly lower in devices with tPA-functionalized brushes when compared to the devices with polymer brushes ($p < 0.05$) as well as the bare devices ($p << 0.001$). This behavior is supported by the corresponding survival curves, where device failure was defined as a 3-fold increase in baseline device resistance (Figure 5b). In 15 min, 83% of the bare devices and 67% of the devices modified with polymer brushes reached the failure criterion, while only 50% of the devices modified with tPA-functionalized polymer brushes failed.

These results are further supported by the quantification of the clot volume using micro-computed tomography (micro-CT, **Figure** 6a), wherein the mean clot volume is lowest in the devices with the tPA-coating system compared to the bare devices and the devices modified with polymer brushes (Figure 6b). These results demonstrate that the tPA-coating system shows a notable improvement in the unwanted formation of clots even in more realistic 3D structures mimicking the geometry and blood flow patterns within oxygenators containing hollow fiber bundles.

3. Conclusion

This study demonstrated the development of a smart hemocompatible surface coating for blood-contacting medical devices that mimics the endothelial regulation of fibrinolysis. This coating system remains dormant in the absence of thrombi but activates in their presence, initiating the fibrinolytic pathway. When applied to 3D printed microchannel devices mimicking the geometry of oxygenator membranes, the coating effectively reduced clot formation. The minimal density of tPA required and the safety of this approach suggest that this strategy is a promising avenue to improve the hemocompatibility of membrane oxygenators and other blood-contacting devices. This self-regulated coating emulates the hemostatic regulation of the endothelium, opening a new paradigm for developing hemocompatible surfaces that autonomously modulate coagulation.

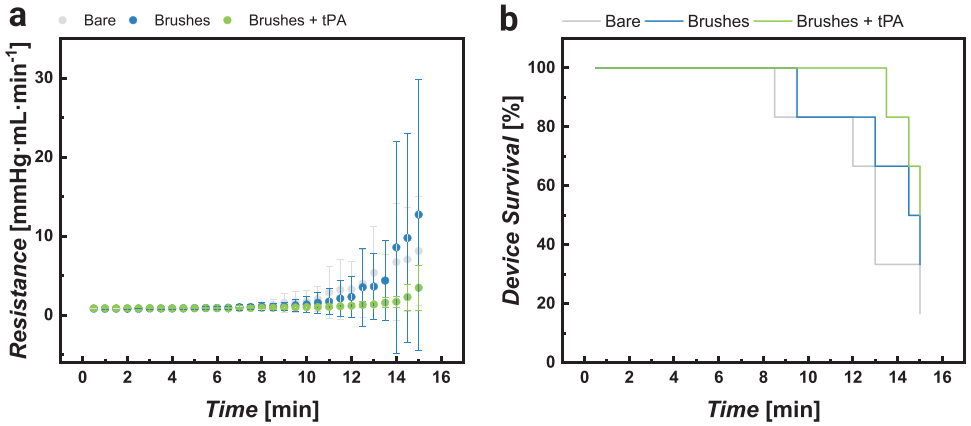

Figure 5. a) Averaged resistance in the microchannel devices during the blood study (15 min) visualizing the difference between the bare device, the device coated with polymer brushes, and the devices coated with tPA-functionalized brushes. (n = 6, each) b) Corresponding survival curves. The threshold is set to 3 times the baseline resistance (≙ 2.46 mmHg·mL·min^{-1}).

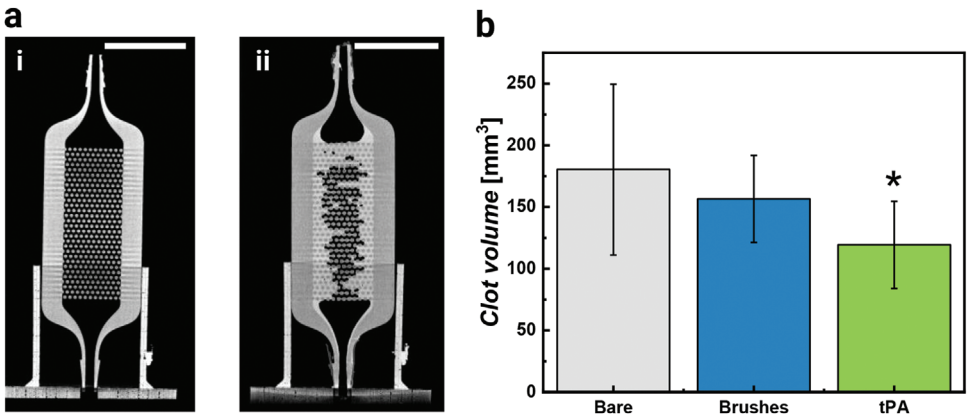

Figure 6. Micro-CT analysis of clot formation. a) Representative micro-CT images of bare device i) before and ii) after blood contact. Scale bars represent 10 mm. b) Clot volume in the bare device, the device coated with polymer brushes, and the devices coated with tPA-functionalized brushes after the blood study. *p-value < 0.05 is considered significant. n = 6.

4. Experimental Section

Materials: All chemicals were used as received and stored appropriately. Plasminogen, chromogenic substrate S-2288 (CS-05(88)) were obtained from CoaChrom Diagnostica GmbH, Austria. *N*-(3-Dimethylaminopropyl)-*N*'-ethylcarbodiimide hydrochloride (EDC, ≥99.0%), and *N*-Hydroxysuccinimide (NHS, >98.0%) were purchased from TCI GmbH, Germany. Citrated BP, copper(II)bromide ($CuBr_2$, 99%), phosphate buffered saline tablets (PBS), boric acid (≥99.5%), and glutaraldehyde were obtained from Sigma Aldrich Chemie GmbH, Germany. Tris(2-dimethylaminoethyl)amine (Me_6TREN, 99+%) was obtained from ThermoFisher GmbH, Germany. DMSO (99.7%), and ethanol (99.8%) were purchased from Acros Organics, Germany. Acetone (99.9%) and sodium hydroxide (pellets) were obtained from Merck KGaA, Germany. SPR-gold-chips were purchased from Cenibra GmbH (BioNavis), Germany. Saline solution (0.9%) was obtained from Fresenius Kabi, Germany. Sodium heparin (25000 I.E per 5 mL) was purchased from ratiopharm GmbH, Germany. 11-(trichloro silyl) undecyl-2-bromo-2-methylpropanoate was synthesized according to literature procedures.[45] *N*-(2-Hydroxypropyl) methacrylamide (HPMA) and (3-methacryloylamino-propyl)-(2-carboxy-ethyl) dimethylammonium (carboxybetaine methacrylamide, CBMAA), were synthesized according to procedures from literature.[46,47]

MethodsX-ray Photoelectron Spectroscopy (XPS): An Ultra AxisTM spectrometer (Kratos Analytical, Manchester, United Kingdom) with a monochromatic A1-Kα source (1486.6 eV) with a total power of 144 W (12 kV x 12 mA) was used to record the XPS spectra. The evaluation of the spectra was performed with the software CasaXPS Version 2.3.22 and the C1s peak of the aliphatic carbon (C—C, C—H) was set to 285.0 eV.

Surface Plasmon Resonance (SPR): SPR measurements were conducted on a two-channel MP-SPR Navi 210A VASA (BioNavis, Tampere, Finland) with BioNavis SPR gold sensor slides using the SPRNavi Control software (Version 4.3.5.2). The results at 670 nm were analyzed via SPR-Navi Data Viewer (Version 4.3.5.2). A conversion factor of 0.0518 ng•cm^{-2} per μRIU was utilized to determine the amounts of proteins.

Initiator Immobilization: Microchannel devices were rinsed three times with ethanol and Milli-Q water and dried with N_2. Subsequently, oxidation with oxygen plasma was performed for 5 min to generate nucleophilic groups at the surface. Afterward, the devices were immersed in a solution of 11-(trichlorosilyl) undecyl-2-bromo-2-methylpropanoate in dry toluene (1 µL·mL^{-1}) for 1 h at 25 °C in an anhydrous atmosphere. The devices were rinsed with toluene, acetone, ethanol, and Milli-Q water and dried with N_2. SPR-Au-chips were rinsed twice with absolute ethanol and Milli-Q water and dried with N_2. Subsequently, the SPR-gold-sensor-slides were spin-coated with the same resin that was used for the fabrication of the microchannel devices and irradiated with UV-light for 30 min. Afterward, the initiator immobilization was carried out in the same way as for the devices.

Grafting of Poly(HPMA-co-CBMAA) Brushes on Microchannel Devices: The copolymerization of HPMA and CBMAA was performed via photoinduced SET-LRP. First, a stock solution of $CuBr_2$ (8.7 mg, 3.9 µmol) and Me_6TREN (62.5 µL, 23.4 µmol) was prepared in 10 mL DMSO. Additionally, HPMA (4.27 g, 30.0 mmol) and CBMAA (1.27 g, 5.27 mmol) were dissolved in DMSO (20.0 mL) in another flask. The stock solution (890 µL) was added to the monomer solution and the obtained polymerization solution was degassed by bubbling with N_2 for 60 min. The microchannel devices were placed in crimped vials and degassed by bubbling with N_2 for 60 min. The degassed polymerization solution (5 mL per vial) was transferred to the vials and the polymerization was conducted by irradiation with a UV-light source (4 × 9 W, λ_{max} = 365 nm) at room temperature. After irradiation for 40 min, the vials were opened and quenched with 5 mL of DMSO to stop the polymerization. The microchannel devices were rinsed with DMSO, ethanol, and Milli-Q water and dried with N_2. The synthesis of the poly(HPMA-*co*-CBMAA) brushes grafted from SPR-gold-sensor-slides was prepared in the same way.

Preparation of Brushes on SPR-Chips: First, a 10 nm-thick resin layer was formed on the SPR-chips by spin-coating the resin followed by 30 min of UV-light irradiation. This step ensures that the surface properties were consistent with those of the devices. Subsequently, the SPR-chips underwent the same procedure as the microchannel devices, including the immobilization of the initiator and the grafting of polymer brushes.

Quantification of the Immobilization of tPA via SPR: Solutions of EDC (76.7 mg, 0.4 M) and NHS (11.5 mg, 0.1 M) were prepared in PBS and only mixed prior to the measurement. The EDC/NHS solution was flushed over the surface for 10 min to activate the carboxylic groups. After activation tPA solutions (20 µg·mL^{-1}) in sodium borate (pH 8.5) were flushed over the surface for 80 min and subsequently washed with PBS or sodium borate to quantify the amount of tPA. The experiments were carried out in triplicate (n = 3).

Antifouling Measurements: The antifouling measurements were carried out using undiluted BP. The surfaces were contacted with BP for 60 min at a flow rate of 10 µL·min^{-1} and the refractive index change was followed by SPR spectroscopy to quantify the amount of adsorbed BP proteins. The experiments were performed in triplicate (n = 3). For the samples with brushes and tPA, the immobilization of tPA was performed directly in the SPR and it was followed by the studies of fouling.

Determining D-Dimer Concentrations in Plasma Samples: To determine the D-Dimer concentration a focused experiment was performed where citrated BP was pumped through the devices with and without surface modification for 30 min with a flow rate of 3 mL·min^{-1}. Afterward, the plasma samples were assayed with an ELISA Kit (ab260076, abcam, Germany) The measurement was carried out in triplicate (n = 3).

Fabrication of Microchannel Devices: The microchannel devices designed in CAD were fabricated using a DLP 3D printer (PR-110, CADworks3D, ON, Canda). The devices had a 2 cm path length with a right-circular cylinder 380 µm in diameter so as to mimic an oxygenator's fiber bundle achieving 50% packing density. A clear microfluidic resin was used (Photopolymer resin Ver. 7.0a, CADworks3D), which was most similar to urethane acrylate plastic with the acrylate monomer constituting over 85% by weight. The printed microchannel devices were rinsed with 60 mL of isopropyl alcohol from both the inlet and outlet barb connectors to remove uncured resin. The device was then post-cured with a UV curing chamber for one min. The volume of the device is 438 µL (20 mm x 7.3 mm x 3 mm).

Microchannel Device Blood Flow Studies: A total of 250 mL of blood was drawn from healthy, non-child-bearing adults weighing over 110 lbs. The blood was slightly anticoagulated upon blood draw with 0.06 $U \cdot mL^{-1}$ heparin and immediately transferred to three 60 mL syringes. Each syringe was connected to an independent flow circuit through 1/16 inch Tygon tubing (Saint-Gobain, Malvern, PA) connected to the microchannel device in a single pass utilizing a syringe pump (New Era Pump Systems Inc., NY, USA). All three circuits were pumped simultaneously at a flow rate of 3 $mL \cdot min^{-1}$. This allowed using the same donor's blood to test one device of each of the three coating groups, hence mitigating donor-induced variability. Digital manometers (CR410, Ehdis, China) were used to measure the pressure difference across the devices every 30 s for a total of 15 min for blood flow resistance measurements. Immediately after the blood draw, plasma-activated partial thromboplastin time (aPTT) was measured (Hemochron Signature Elite, Werfen, Spain) and 350 µL blood was collected in a microtainer coated with K_2EDTA (BD, NJ, USA) for complete blood count measurements (Genesis, Oxford Science). Experimental data was not used if plasma aPTT was not between 30–45 s or if hematocrit was below 40%. The devices were detached from the circuit and promptly flushed with heparinized saline (2 $U \cdot mL^{-1}$) to arrest further clot formation. Fixation of the clot was performed with 4 w% paraformaldehyde for 2°h at room temperature following which they were imaged with µ-CT. Since the volume of the device is small compared to the syringe that serves as a blood container and the residence time is only 8.8 s, this experiment was focused on the device itself and not on the different markers in blood. The microchannel flow studies were approved by the Institutional Review Board of Carnegie Mellon University, Pittsburgh (IRB ID: STUDY2021_00000488), and informed written consent of all participants was obtained. This experiment was repeated six times using a different donor for each experiment.

Clot Volume Quantification with Micro-CT: All three devices from each blood study were scanned concurrently in a purpose-built device holder after the fixation step. Micro-CT scans for four of the six studies were conducted using Skyscan 1172 (Bruker-Skyscan, Contich, Belgium) while devices from two studies were imaged using Xradia CrystalCT (Zeiss, Oberkochen, Germany). Imaging with SkyScan 1172 was done with a source voltage of 40 kV at 250 µA and a 0.5s exposure, 6 frame averaging with 2 × 2 binning resulting in a 13.45 µm voxel size. Scans with the Xradia Crystal CT were carried out with a 0.4s per frame exposure, 5 frames averaging at 50 kV and 4 W with no pixel binning achieving a 10 µm voxel size. No source filter was used while capturing the projections from either instrument. The obtained 16-bit data was analyzed for clot volume using Dragonfly (Object Research Systems, Québec, Canada).

Statistical Analyses: The measured clot volume and flow resistance data were analyzed with SPSS (International Business Machines Corporation, NY, USA) to study statistical significance amongst the coating groups. Device clot burden was studied using a linear mixed effects model wherein the natural logarithm of clot volume was the dependent variable. The donor ID was the subject variable, coating (i.e., device type) as a fixed effect and plasma aPTT was a covariate. The model also accounted for the interaction of device type and aPTT. Resistance time series data was analyzed using a generalized linear mixed effects model. Measured resistance was the dependent variable with time as the repeated measures condition. The model incorporated device coating, time, aPTT, and their interactions while the Donor ID was specified as a random effect. Bonferroni correction was used to adjust the p values of both model outcomes.

Supporting Information

Supporting Information is available from the Wiley Online Library or from the author.

Acknowledgements

The authors acknowledge the financial support by the German Federal Ministry of Education and Research (BMBF) with the project Heart2.0 within the "Bio4MatPro-Competence Center for Biological Transformation of Materials Science and Production Engineering" program (grant no. 031B1154B), the Deutsche Forschungsgemeinschaft (DFG, German Research Foundation) via Schwerpunktprogramm "Toward an Implantable Lung" (Project number: 346972946), the European Innovation Council (EIC) under the European Union's Horizon Europe program, IV-Lab, project number: 101115545, and IBEC which is a member of the CERCA Programme/Generalitat de Catalunya. The microchannel flow studies were approved by the Institutional Review Board of Carnegie Mellon University, Pittsburgh (IRB ID: STUDY2021_00000488), and informed written consent of all participants was obtained. A portion of this research was sponsored by the Army Research Laboratory and was accomplished under Cooperative Agreement Number W911NF-20-2-0175. The views and conclusions contained in this document were those of the authors and should not be interpreted as representing the official policies, either expressed or implied, of the Army Research Laboratory or the U.S. Government. The U.S. Government is authorized to reproduce and distribute reprints for Government purposes notwithstanding any copyright notation herein. The authors also thank Isaac Swink for assistance with micro-CT analysis.

Open access funding enabled and organized by Projekt DEAL.

Conflict of Interest

The authors declare no conflict of interest.

Data Availability Statement

The data that support the findings of this study are available from the corresponding author upon reasonable request.

Keywords

antifouling polymer brushes, extracorporeal membrane oxygenator, fibrinolytic coating, 3D printing, tissue plasminogen activator

Received: October 29, 2024
Revised: January 2, 2025
Published online: January 13, 2025

[1] H. E. Achneck, B. Sileshi, A. Parikh, C. A. Milano, I. J. Welsby, J. H. Lawson, *Circulation* **2010**, *122*, 2068.
[2] I. Reviakine, F. Jung, S. Braune, J. L. Brash, R. Latour, M. Gorbet, W. van Oeveren, *Blood Rev.* **2017**, *31*, 11.
[3] I. H. Jaffer, J. C. Fredenburgh, J. Hirsh, J. I. Weitz, *J. Thromb. Haemostasis* **2015**, *13*, S72.
[4] J. I. Weitz, *Am. J. Hematol.* **2012**, *87*, S133.
[5] D. Gustafsson, R. Bylund, T. Antonsson, I. Nilsson, J. E. Nystrom, U. Eriksson, U. Bredberg, A. C. Teger-Nilsson, *Nat. Rev. Drug Discovery* **2004**, *3*, 649.
[6] J. C. Fredenburgh, J. I. Weitz, *J. Thromb. Haemostasis* **2021**, *19*, 20.

[7] M. N. Levine, J. Hirsh, S. Landefeld, G. Raskob, *Chest* **1992**, *102*, 352S.
[8] J. D. Andrade, V. Hlady, *Ann. N. Y. Acad. Sci.* **1987**, *516*, 158.
[9] J. D. Andrade, V. L. Hlady, R. A. Van Wagenen, *Pure Appl. Chem.* **1984**, *56*, 1345.
[10] T. Chandy, G. S. Das, R. F. Wilson, G. H. R. Rao, *Biomaterials* **2000**, *21*, 699.
[11] C. M. G. Carlsson, K. S. Johansson, *Surf. Interface Anal.* **1993**, *20*, 441.
[12] A. Vesel, M. Mozetic, *Vacuum* **2012**, *86*, 634.
[13] R. Lorusso, G. De Cicco, P. Totaro, S. Gelsomino, *Interact. Cardiovasc. Thorac. Surg.* **2009**, *8*, 7.
[14] M. Tanaka, T. Motomura, M. Kawada, T. Anzai, Y. Kasori, T. Shiroya, K. Shimura, M. Onishi, A. Mochizuki, *Biomaterials* **2000**, *21*, 1471.
[15] S. Gunaydin, B. Farsak, M. Kocakulak, T. Sari, C. Yorgancioglu, Y. Zorlutuna, *Ann. Thorac. Surg.* **2002**, *74*, 819.
[16] K. L. Prime, G. M. Whitesides, *J. Am. Chem. Soc.* **1993**, *115*, 10714.
[17] M. Mrksich, G. B. Sigal, G. M. Whitesides, *Langmuir* **1995**, *11*, 4383.
[18] P. Harder, M. Grunze, R. Dahint, G. Whitesides, P. Laibinis, *J. Phys. Chem. B* **1998**, *102*, 426.
[19] M. E. McGovern, *Anal. Commun.* **1998**, *35*, 391.
[20] R. S. Kane, P. Deschatelets, G. M. Whitesides, *Langmuir* **2003**, *19*, 2388.
[21] R. C. Advincula, W. J. Brittain, K. C. Caster, J. Rühe, *Polymer Brushes: Synthesis, Characterization, Applications*, Wiley Interscience, Hoboken, New Jersey **2004**.
[22] A. Halperin, *Langmuir* **1999**, *15*, 2525.
[23] M. Krishnamoorthy, S. Hakobyan, M. Ramstedt, J. E. Gautrot, *Chem. Rev.* **2014**, *114*, 10976.
[24] C. Arnander, M. Dryjski, R. Larsson, P. Olsson, J. Swedenborg, *J. Biomed. Mater. Res.* **1986**, *20*, 235.
[25] O. Larm, R. Larsson, P. Olsson, *Biomater., Med. Devices, Artif. Organs* **1983**, *11*, 161.
[26] S. Gore, J. Andersson, R. Biran, C. Underwood, J. Riesenfeld, *J. Biomed. Mater. Res., Part B* **2014**, *102*, 1817.
[27] H. P. Wendel, G. Ziemer, *Eur. J. Cardiothorac. Surg.* **1999**, *16*, 342.
[28] G. Johnson, B. Curry, L. Cahalan, R. Prater, J. Biggerstaff, A. Hussain, M. Gartner, P. Cahalan, *Perfusion* **2013**, *28*, 263.
[29] M. C. Wyers, M. D. Phaneuf, E. M. Rzucidlo, M. A. Contreras, F. W. LoGerfo, W. C. Quist, *Cardiovasc. Pathol.* **1999**, *8*, 153.
[30] J. C. Lin, S. M. Tseng, *J. Mater. Sci.: Mater. Med.* **2001**, *12*, 827.
[31] M. Akashi, I. Maruyama, N. Fukudome, E. Yashima, *Bioconjugate Chem.* **1992**, *3*, 363.
[32] C. Sperling, K. Salchert, U. Streller, C. Werner, *Biomaterials* **2004**, *25*, 5101.
[33] J. Yu, E. Brisbois, H. Handa, G. Annich, M. Meyerhoff, R. Bartlett, T. Major, *J. Mater. Chem. B* **2016**, *4*, 2264.
[34] R. C. Jin, J. Loscalzo, *J. Blood Med.* **2010**, 147.
[35] M. Ashcraft, M. Douglass, Y. Chen, H. Handa, *Biomater. Sci.* **2021**, *9*, 2413.
[36] F. Obstals, L. Witzdam, M. Garay-Sarmiento, N. Y. Kostina, J. Quandt, R. Rossaint, S. Singh, O. Grottke, C. Rodriguez-Emmenegger, *ACS Appl. Mater. Interfaces* **2021**, *13*, 11696.
[37] B. Wiman, D. Collen, *Nature* **1978**, *272*, 549.
[38] U. Christensen, I. Clemmensen, *Biochem. J* **1977**, *163*, 389.
[39] M. Hoylaerts, D. C. Rijken, H. R. Lijnen, D. Collen, *J. Biol. Chem.* **1982**, *257*, 2912.
[40] K. Woodhouse, J. Weitz, J. Brash, *Biomaterials* **1996**, *17*, 75.
[41] E. Angles-Cano, *Chem. Phys. Lipids* **1994**, *67–68*, 353.
[42] V. Fleury, E. Angles-Cano, *Biochemistry* **1991**, *30*, 7630.
[43] N. Umei, A. Lai, J. Miller, S. Shin, K. Roberts, S. A. I. Qatarneh, S. Ichiba, A. Sakamoto, K. E. J. J. o. T. M. Cook, *J. Transl. Med.* **2021**, *19*, 179.
[44] A. Lai, N. Omori, J. E. Napolitano, J. F. Antaki, K. J. b. Cook, *bioRxiv* **2024**, *5*, 574443.
[45] M. Vorobii, A. de los Santos Pereira, O. Pop-Georgievski, N. Y. Kostina, C. Rodriguez-Emmenegger, V. Percec, *Polym. Chem.* **2015**, *6*, 4210.
[46] K. Ulbrich, V. Šubr, J. Strohalm, D. Plocova, M. Jelınková, B. Řıḥová, *J. Controlled Release* **2000**, *64*, 63.
[47] N. Y. Kostina, C. Rodriguez-Emmenegger, M. Houska, E. Brynda, J. í. Michálek, *Biomacromolecules* **2012**, *13*, 4164.